Crystalline Homopolyimides and Copolyimides Derived from 3,3′,4,4′-Biphenyltetracarboxylic Dianhydride/ 1,3-Bis(4-aminophenoxy)benzene/1,12-Dodecanediamine. 2. Crystallization, Melting, and Morphology

Benjamin S. Hsiao* and John A. Kreuz†

Experimental Station, Central Research and Development, E. I. du Pont de Nemours & Company, Wilmington, Delaware 19880

Stephen Z. D. Cheng

Institute of Polymer Science, The University of Akron, Akron, Ohio 44325

Received April 4, 1995; Revised Manuscript Received October 11, 1995[⊗]

ABSTRACT: A study of crystallization, melting, and morphology is carried out for homopolyimides derived from 3,3′,4,4′-biphenyltetracarboxylic dianhydride (BPDA) and either 1,3-bis(4-aminophenoxy)benzene (134APB) or 1,12-dodecanediamine (C12), as well as copolyimides containing different compositions of 134APB and C12. For copolyimides, although a singular glass transition was seen in each composition, the crystallization and melting behavior of all compositions is dominated by either 134APB/BPDA or C12/BPDA homopolyimide crystals. The bulk crystallization rate is significantly reduced in compositions with high C12 content. Compositions of copolyimides with 40/60 and 20/80 134APB/C12 ratios additionally exhibited dual maxima in crystallization rates which can be attributed to the phase separation of the two crystals. Since no large depression in the spherulite growth rate was found, the decrease in the bulk crystallization rate is primarily due to the decrease in nucleation density. The last endotherm in the triple-melting behavior is associated with a reorganization process rather than the polymorphism, as verified by DSC and X-ray diffraction. Finally, two major spherulite appearances were identified: (1) Maltese-cross spherulites with negative birefringence in 134APB/BPDA dominant systems; (2) ringed-like spherulites with no preferred birefringence in C12/BPDA dominant systems. Both morphologies consist of lamellar crystals with the 134APB/BPDA crystals having a broader thickness than C12/BPDA, as was determined by small angle X-ray scattering.

Introduction

Previously, we have synthesized a copolyimide family containing 3,3′,4,4′-biphenyltetracarboxylic dianhydride (BPDA) and either 1,3-bis(4-aminophenoxy)benzene (134APB) or 1,12-dodecanediamine (C12) diamines.[1] The chemical structures of the two homopolyimides 134APB/BPDA and C12/BPDA are as follows:

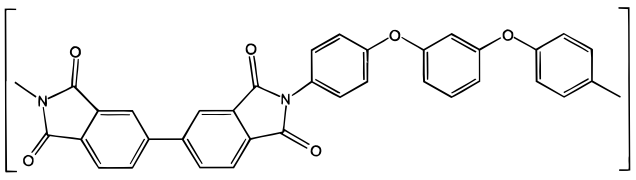

134APB/BPDA

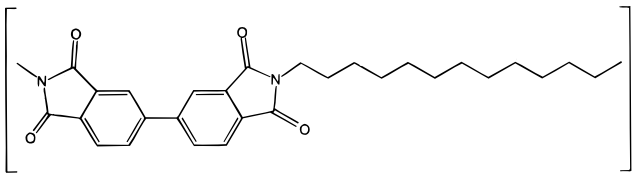

C12/BPDA

These copolymers have a wide range of singular glass transition and equilibrium melting temperatures. They can serve as a model system enabling us to understand the structure/crystallization/morphology relationships in thermoplastic copolyimides containing both rigid aromatic and flexible alkyl portions. A similar copolyimide system containing 4,4′-oxydiphthalic anhydride (ODPA) and a flexible ethylene glycol sequence has recently been studied by Cheng *et al.*[2−4]

The two homopolyimides, 134APB/BPDA and C12/BPDA, are crystallizable but have distinctly different thermal properties and thus melt processibilities. For instance, 134APB/BPDA has a T_g at 220 °C and a $T_m°$ (equilibrium melting temperature) at 410 °C that is near the thermal degradation temperature, whereas C12/BPDA has a lower T_g at 80 °C and a $T_m°$ at 243 °C.[1] We have demonstrated that copolymerization is an effective method to control the relationships between T_g and $T_m°$, and possibly other physical properties.

The use of copolymerization with two different crystallizing segments to tailor thermal/mechanical properties has been widely adopted. Many examples can be found in polymer textbooks.[5−8] In the chosen 134APB/C12//BPDA system, the appearance of a singular T_g indicates that the material is homogeneous in all compositions in its amorphous state. Since no evidence of cocrystallization can be found by X-ray techniques, the crystalline behavior of different copolymers is a function of composition and degree of supercooling.

In this work, detailed analysis is carried out to study the crystallization, melting, and morphology of these homo- and copolyimides. The crystallization study includes the bulk crystallization rate measured by differential scanning calorimetry (DSC) and the spherulitic crystal growth rate measured by thermal optical analysis (TOA). The interesting phenomenon of triple-melting behavior[1] is investigated by altering the heating rate in DSC and by the X-ray diffraction study of

* To whom correspondence should be addressed.
† DuPont High Performance Films, Circleville, OH.
⊗ Abstract published in *Advance ACS Abstracts,* December 1, 1995.

0024-9297/96/2229-0135$12.00/0

annealed specimens. The morphology is characterized on two length scales: (1) the spherulite appearance around the micrometer dimension using polarizing light microscopy and transmission electron microscopy (of the etched surfaces) and (2) the lamellar information around the nanometer dimension using small-angle X-ray scattering (SAXS) and correlation function methods. The detailed crystal structural analysis will be carried out from polymer fiber X-ray patterns, which will be discussed in a future paper.

Experimental Section

Materials and Preparation. The chemical composition and molecular weight information of the chosen system have been described in a previous paper.[1] All samples were vacuum dried at 100 °C for 24 h prior to any preparation and measurements. Thin films (thickness about 5 μm) were prepared by melt pressing powder specimens at approximately 10 deg above $T_m°$ for thermal optical microscopy analysis. Crystalline samples were prepared by isothermal annealing at different temperatures above T_g for at least 1 h, which were used in DSC heating rate analysis and X-ray studies (WAXD and SAXS). The permanganic etching was performed as follows. A solution of 50 mL of concentrated sulfuric acid, 30 mL of 85% phosphoric acid, and 2 g of ground potassium permanganate was well mixed for 15 min with 10 mL of distilled water. The specimen was immersed in this solution for about 15 min in an ultrasonic bath to prevent redeposition of degraded polymer. The recovered specimens were then rinsed with distilled water and air dried. Etched specimens were exposed to a carbon−platinum vapor at a low angle in a vacuum evaporator, followed by coating with a poly(acrylic acid) solution, and allowed to dry. The dry replica was stripped and vacuum evaporated with carbon. The poly(acrylic acid) coating was dissolved by overnight soaking onto the surface of water in a Petri dish. This left behind the replica which was picked up on copper meshed grids, dried, and transferred to the electron microscope.

Characterization Techniques. A Perkin-Elmer DSC7 was used to carry out the isothermal crystallization kinetics and different heating rate studies (10−150 °C/min). In the former, the sample was first equilibrated at about 10 deg above their $T_m°$ for 10 min and then fast cooled at a 320 °C/min rate to different temperatures for the measurement. All thermal scans were taken under a nitrogen environment. The isothermal crystallization peak time was recorded to characterize the crystallization rate (inversely proportional to the peak time).

The transmission electron microscopy (TEM) work was carried out on a JEOL 2000FX, and images were obtained at a 120 kV accelerating voltage and recorded on sheet films. The optical microscope used was a polarizing Nikon Optiphot-PDL model equipped with a 35 mm camera/video image analyzer and a Mettler FP82 HT hot stage. A first-order red tint plate was used to determined the sign of the spherulitic birefringence under crossed polarizers. Video image analyzing software "JAVA" (Jandel Scientific, CA) was used to determine the spherulitic growth rate.

Wide-angle X-ray diffraction (WAXD) of a powder sample was carried out via an automated Philips diffractometer with Cu Kα radiation. Data were collected in a fixed time mode with a step size of 0.05° (2θ) and run from $2\theta = 4$ to 65°. Small-angle X-ray scattering (SAXS) measurements were conducted using Kratky optics (slit size 120 μm) with a scintillation counter and Cu Kα radiation. The data were collected in a step size of 0.01° (2θ) from $2\theta = 0.12$ to 4°. No desmearing procedure was carried out. The scattering data were corrected for the sample thickness, absorption, and thermal density fluctuation using Porod's law: $\hat{I}(q) = I_b + K/q^3$, where $\hat{I}(q)$ is the smeared scattering intensity, $q = 4\pi \sin(\theta)/\lambda$, θ is the scattering angle, λ is the wavelength, I_b represents the electron density fluctuation, and K is the Porod's asymptote.[9] The correlation function $\gamma(r)$ was then calculated by

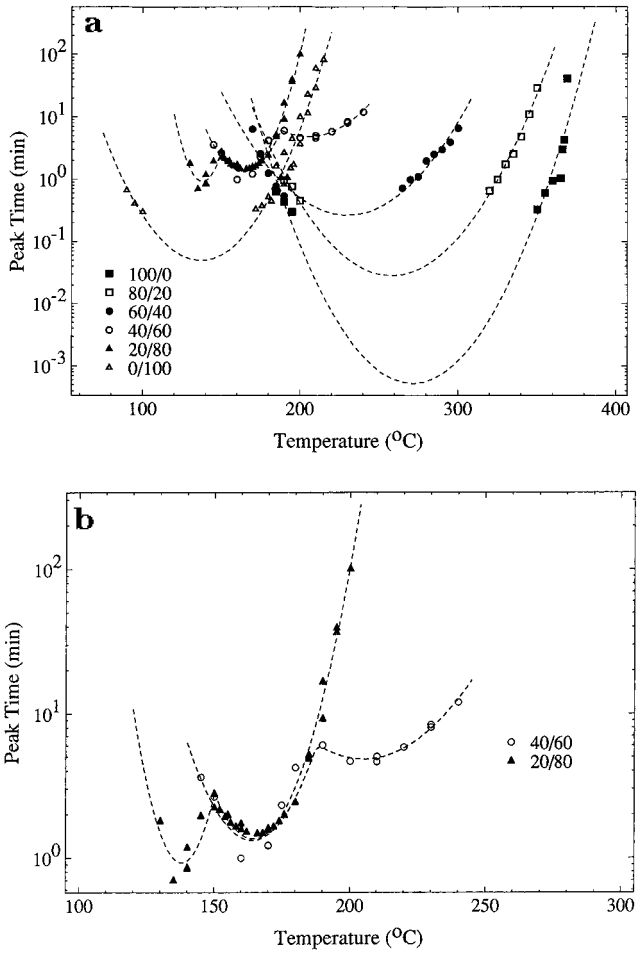

Figure 1. Crystallization peak time *vs* temperature plot: (a) polymers containing different 134APB/C12 compositions from 100/0 to 0/100; (b) the two minima in peak time in compositions of 40/60 and 60/40. The dotted lines represent the second-order polynomial fits.

$$\gamma(r) = (1/4\pi^2)\int_0^\infty (\hat{I}(q) - I_b)q[J_o(qr) - (qr)J_1(qr)]\,dq \quad (1)$$

where the intensity was extrapolated to $q = \infty$ using the Porod law and to $q = 0$ by using $Iq = 0$ at the origin. Four lamellar variables were estimated from $\gamma(r)$:[10] long period L, linear degree of crystallinity x_{CL}, invariant Q, and lamellar thickness l_C as the product of L and x_{CL}.

Results and Discussion

Crystallization Kinetics. The crystallization peak time *vs* temperature plot for homo- and copolyimides containing different 134APB/C12 ratios is shown in Figure 1a. (The peak time is associated with the half-time and is also inversely proportional to the crystallization rate). In this figure, two sets of kinetics behavior are identified: the first set (100/0 to 40/60) dominated by the 134APB/BPDA crystal, and the second one (20/80 to 0/100) dominated by the C12/BPDA crystal. In the first set, the peak time is found to increase with increasing C12 content. The increase is over 1 order of magnitude in minute for every 20% of diamine ratio change. In addition, the maximum crystallization rate temperature, where the plot of peak time *vs* temperature shows a minimum, is shifted to a lower value with increasing C12. In contrast, the C12/BPDA dominant system (20/80 and 0/100) shows an increase with the similar magnitude in peak time as the 134APB content increases.

A close examination of Figure 1a reveals that both 20/80 and 40/60 compositions exhibit dual minima in

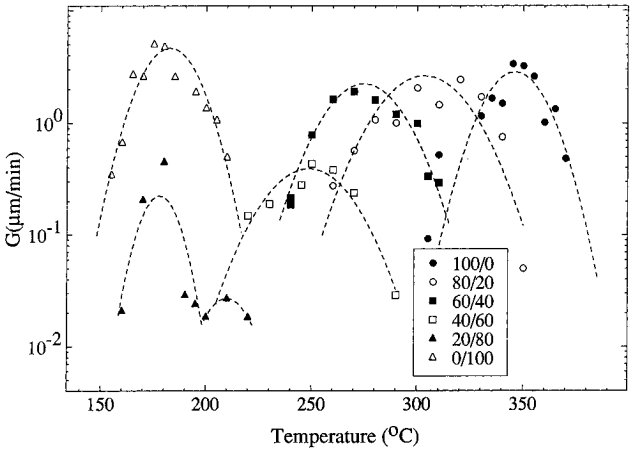

Figure 2. Linear spherulite growth rate *vs* temperature diagram for polymers containing different 134APB/C12 compositions from 100/0 to 0/100. The dotted lines also represent the second-order polynomial fits.

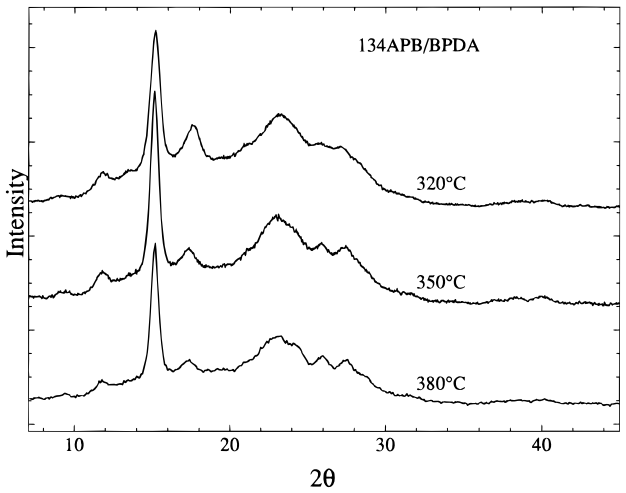

Figure 3. WAXD powder patterns of 134APB/BPDA samples crystallized at 320, 350, and 380 °C.

peak time (the enlarged diagram shown in Figure 1b). Furthermore, the high-temperature curve in 20/80 is identical to the lower temperature curve in 40/60. It is conceivable the dual minima in peak time are results of crystallization from two incompatible crystalline phases. In other words, this observation is due to the crystallization-induced phase separation between 134-APB/BPDA and C12/BPDA crystals (thus, the copolymers may not be totally random). Such an argument is certainly consistent with the range of the peak time window observed for each composition. For instance, the peak time window for 134APB/BPDA is between 170 and 380 °C, and for C12/BPDA is between 80 and 230 °C. The two windows intercept at approximately 190 °C, which is near the break point of the dual-minimum curve in 40/60. Thus, in 40/60, the high-temperature curve (above 190 °C) probably represents the crystallization of the 134APB/BPDA-dominated phase, and the low-temperature curve represents the crystallization of the C12/BPDA-dominated phase. However, the dual minima in 20/80 must be assigned otherwise: the high-temperature curve probably still represents the C12/BPDA crystallization in a 134APB/BPDA-enriched phase, which is identical to the low-temperature curve in 40/60, whereas the low-temperature curve represents the C12/BPDA-crystallization in a C12/BPDA enriched phase.

The linear spherulitic growth rate (G) for different 134APB/C12 compositions measured at varying temperatures is shown in Figure 2 (the symbols represent the experimental data and the dotted lines represent the second-order polynomial fits). These data were determined in the linear growth period prior to the spherulite impingement. It is seen that the values of G for different compositions are quite similar (but in different temperature ranges), except for the compositions of 40/60 and 20/80 where lower rates are seen. These results are very different from the observation of crystallization peak time where 1 order of magnitude difference in peak time for each composition was seen. In Figure 2, the maximum growth rate temperature, at which the spherulitic growth rate is the fastest, is found to shift to a lower temperature with increasing C12. This shift is somewhat similar to the shift of the maximum crystallization rate temperature in Figure 1. In the composition of 20/80, a double maximum growth rate behavior is also observed. This phenomenon is due to the growth of two different types of spherulites which will be discussed later.

The marked difference between the large change in crystallization peak time and the small change in G in compositions from 100/0 to 60/40 suggests that the nucleation density must be responsible for the reduction in bulk crystallization rate. (The bulk crystallization rate is a combination of the linear growth rate and the rate of nucleation density.[11]) This is reasonable because if the two crystallizing components cannot cocrystallize (as verified by X-ray studies, see below), the demixing process in the copolymer system can significantly hamper the nucleation formation. It is conceivable that the nucleation density is high in either of the two homopolyimides and substantially lower in the copolyimides. Furthermore, we believe that the nucleation density in 134APB/BPDA should be higher than that in C12/BPDA, since the former has a faster bulk crystallization rate but a compatible growth rate as compared to the latter.

Triple-Melting Behavior. In the previous study,[1] we have shown that all compositions (100/0 to 0/100) exhibited a triple-melting behavior if annealed at lower crystallization temperatures and exhibited a conventional double-melting behavior when annealed at higher temperatures. Apparently, the triple-melting behavior is not due to the melting of different crystallized compositions, at least not in the two homopolyimides since they only contain a single component. One possibility is that it is due to the melting of different crystal forms (polymorphs). To test this hypothesis, we have prepared crystalline samples for the two homopolymers annealed at different temperatures which showed both triple-melting and double-melting behavior. The X-ray diffraction powder patterns of these samples (134APB/BPDA and C12/BPDA) are shown in Figures 3 and 4, respectively. Although the high-temperature annealing generally produces a relatively perfect crystalline structure (sharper and more defined peaks, as in Figure 4), the peak occurrence and their positions are found to be independent of crystallization temperature. This indicates that the triple-melting behavior is probably not due to the polymorphism. (The crystal unit cell structure will be discussed in a future publication.)

Another possibility for the triple-melting behavior is associated with the recrystallization/reorganization process during heating. This phenomenon has been observed in poly(aryl ether ketone ketone) containing a 16.7% molar ratio of an isophthalic moiety (PEKK 50/50),[12] which was verified by changing the scanning rate

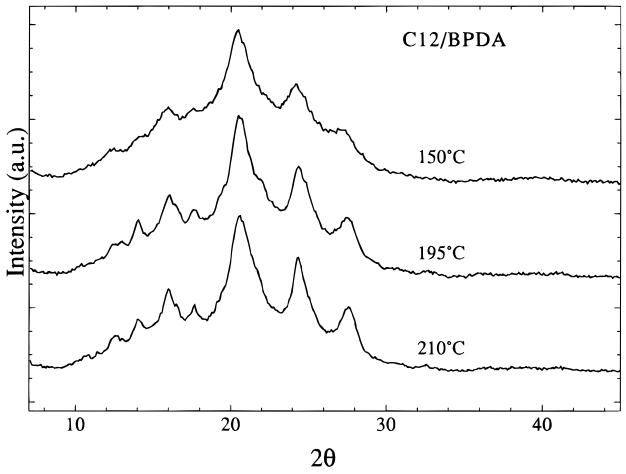

Figure 4. WAXD powder patterns of C12/BPDA samples crystallized at 150, 195, and 210 °C.

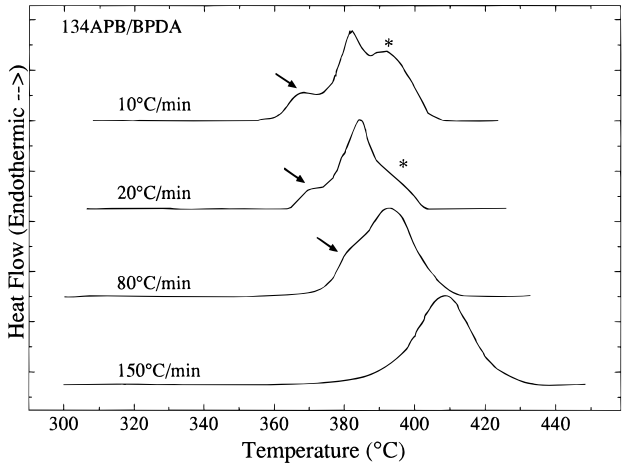

Figure 5. Effect of heating rate on the triple-melting behavior. The chosen sample was 134APB/BPDA crystallized at 360 °C. (The scale of the heat flow was arbitrarily adjusted for comparison.)

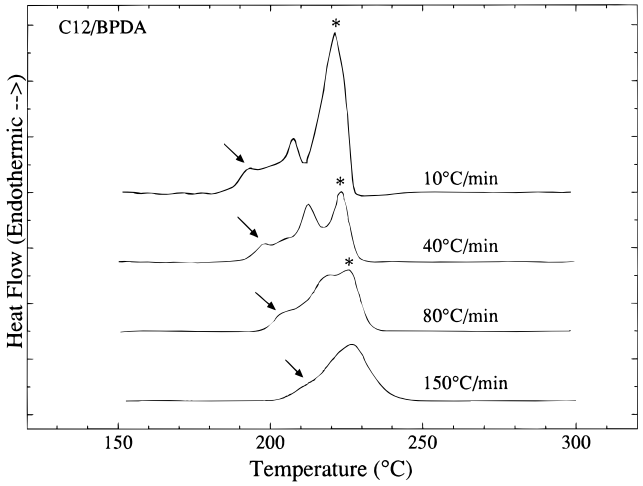

Figure 6. DSC scans of the C12/BPDA sample crystallized at 180 °C at different heating rates. (The scale of the heat flow was arbitrarily adjusted for comparison.)

in DSC. The DSC heating scans of both crystalline homopolymers exhibiting the triple-melting behavior run at different scanning rates are shown in Figures 5 and 6 (134APB/BPDA was annealed at 360 °C and C12/BPDA annealed at 180 °C). It is seen that the last endotherm (marked by the asterisk) vanishes rapidly

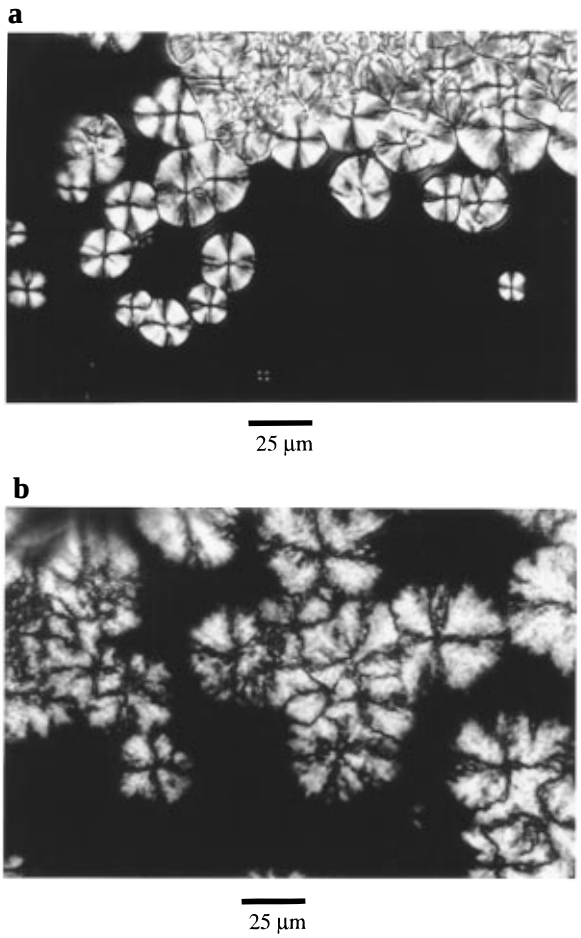

Figure 7. Typical polarizing optical micrographs of Maltese-cross spherulites with negative birefringence from 134APB/BPDA samples: (a) spherulites formed at 340 °C; (b) spherulites formed at 365 °C.

with the increasing heating rate, whereas the lower two endotherms remained relatively stable. Thus, we conclude that the highest endotherm of the triple-melting behavior is due to the reorganization process and the two lower endotherms share the same origin as the conventional double-melting behavior. This finding also supports our extrapolation of the equilibrium melting temperature using the middle endotherm peak temperature as the nominal melting point.[1]

Morphology. Spherulite morphology was found in all compositions. However, the presence of different spherulite types depends on the composition as well as the crystallizing temperature. In summary, three types of spherulites have been identified. In the 134APB/BPDA dominant systems (100/0 to 40/60), the major type is the Maltese-cross pattern with a negative birefringence. The negative birefringence was determined by optical polarizing microscopy using a red one-wavelength plate,[13] which was persistent throughout the measured temperature range. The observation of the negative birefringence indicates that the refractive index along the radial spherulite direction is smaller than the refractive index along the tangential direction. Since the polarizability of the 134APB/BPDA chain along the chain axis is expected to be larger than the perpendicular ones, the spherulite growth direction should coincide with the direction perpendicular to the chain axis. The detailed molecular arrangement within the spherulite will be studied by electron diffraction in the future.

Two typical negative spherulites for 100/0 formed at different temperatures are shown in Figure 7a,b. Al-

though both spherulites are negative in birefringence, the texture of each spherulite is a function of crystallizing temperature. It is seen that at lower temperatures (Figure 7a), the spherulites exhibit a smooth but consistent periphery, whereas at higher temperatures (Figure 7b), the spherulites exhibit a jagged and rough periphery. The difference in these spherulite appearances can be explained by the nucleation theory as follows. It is known that, at lower crystallization temperatures, a fast secondary nucleation formation usually occurs which would lead to a smooth periphery. In contrast, the high-temperature crystallization often results in a slow secondary nucleation rate that leads to a rough periphery. A similar phenomenon has been reported in many semicrystalline polymers before.[11]

The constituent of the observed negative spherulites is the lamellar crystal, which can be visualized by transmission electron microscopy. A typical TEM image of the etched surface from the 134APB/BPDA spherulites is shown in Figure 8a, in which fine lamellar textures are clearly identified. These lamellae have an average thickness of about 10 nm, and the center of each spherulite consists of a sheath-like texture (Figure 8b). Such a morphology is also similar to some other semicrystalline systems such as poly(aryl ether ketones).[12,14−16]

The average lamellar thickness can be more precisely determined by small-angle X-ray scattering (SAXS). SAXS patterns (with smeared intensity) taken from crystalline 134APB/BPDA samples annealed at different temperatures are shown in Figure 9. A scattering maximum is consistently seen in all samples, which can be attributed to the long period repeat from a crystalline/amorphous two-phase stacking morphology. The corresponding correlation functions from SAXS data calculated by eq 1 are shown in Figure 10. From these functions, we have calculated the long period L, linear degree of crystallinity x_{CL}, normalized invariant Q, and lamellar thickness l_C which is defined as the product of L and x_{CL}. The results are listed in Table 1. It is seen that the long period is about 14 nm, which is much smaller than the value calculated from the scattering maximum using Bragg's law. This is expected, which indicates the heterogeneity in the population of two-phase stacking.[10] The linear degree of crystallinity is about 70%, that was determined with the assistance of the crystallinity index (about 35%) by WAXD. It is seen that the calculated lamellar thickness slightly increases with annealing temperature, which has a value from 10 to 12 nm that is similar to the value determined by TEM. The invariant Q shows a maximum value for the sample crystallized at 350 °C, which is near the maximum growth rate temperature (Figure 2). If we assume the crystal and amorphous density contrast remains unchanged, the large value in Q may be attributed to the increase in the total degree of crystallinity.

In addition to the Maltese-cross spherulites, aggregate-like spherulites are also found to be coexistent at temperatures near the maximum growth rate range. However, this morphology can only be observed in 100/0 and 80/20. They have no preferred optical orientation but a faster growth rate (1.5−3 times faster than the coexisting negative spherulites). Note that the growth rate in Figure 2 was determined only from the negative spherulites rather from the aggregates. Similar aggregate morphology has also been observed in nylon 66 before.[17,18] We believe the aggregates are associated with the change in the crystal growth habit induced by the large elastic strain in the amorphous phase. This phenomenon needs to be further investigated in the future.

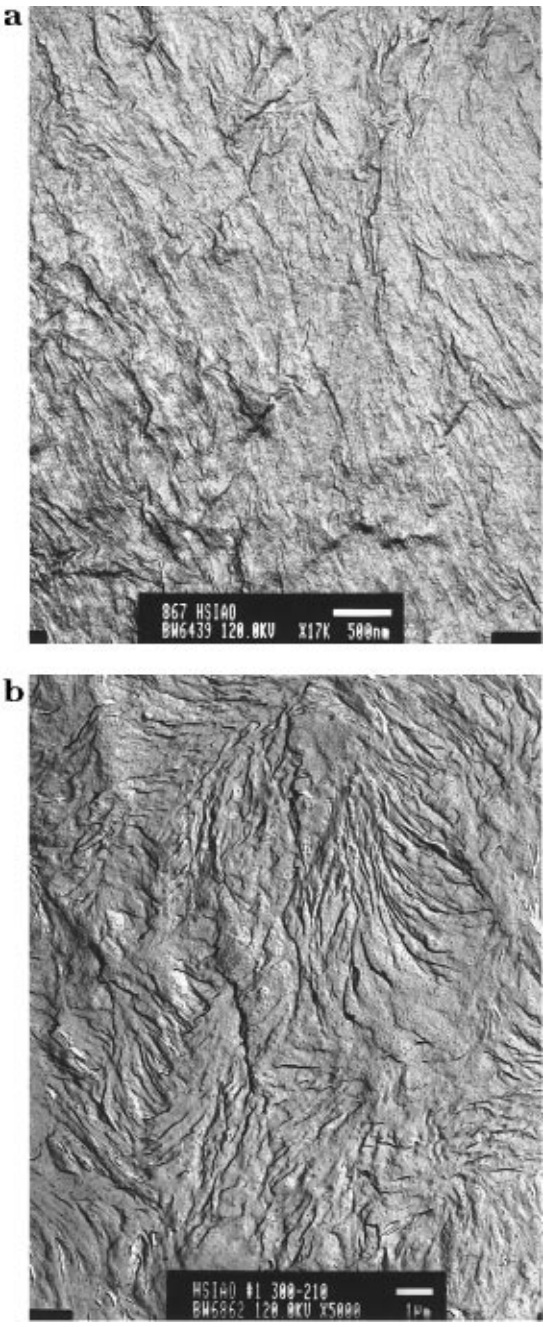

Figure 8. TEM micrographs of replicas from etched 134APB/BPDA surfaces (crystallized at 350 °C): (a) higher resolution showing the fine lamellae; (b) lower resolution showing the sheath-like texture in the spherulite core.

Parts a and b of Figure 11 show two typical ringed spherulites in the C12/BPDA dominant systems (20/80 and 0/100) crystallized at different temperatures. The ringed spherulites were also found in 40/60 and 60/40 but only at higher crystallization temperatures. The spacing between the ring was found to be a function of crystallization temperature. At lower temperatures, the ring spacing is generally narrower; at higher temperatures, the ring spacing becomes wider and less apparent. The sign of birefringence in these spherulites cannot be identified. Nevertheless, its optical orientation is not totally random as for the aggregates. In fact, no aggregate-like spherulite has ever been seen in these compositions. The ringed textures are relatively regular

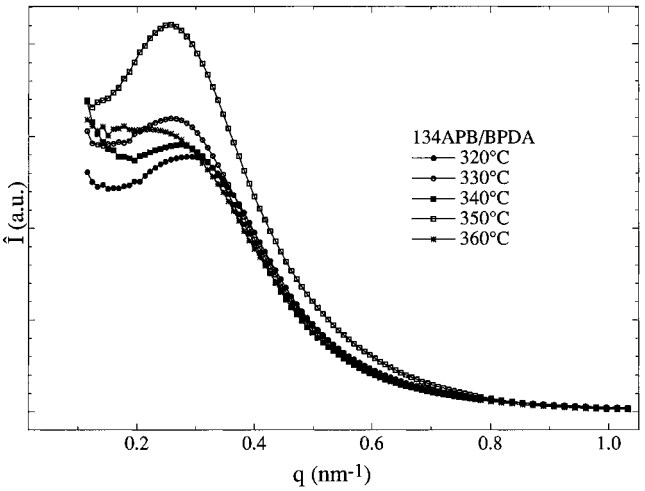

Figure 9. SAXS patterns (with smeared intensity) taken from 134APB/BPDA samples crystallized at different temperatures.

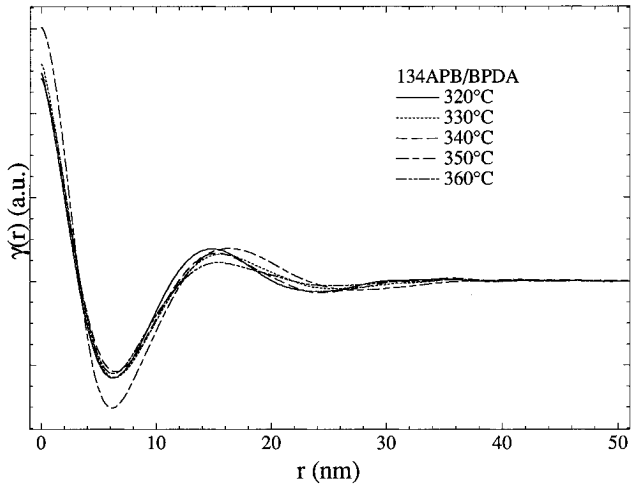

Figure 10. Corresponding correlation function diagrams calculated from Figure 9.

Table 1. Lamellar Variables Calculated by Correlation Functions $\gamma(r)$ (Figure 10) from 134APB/BPDA Samples Crystallized at Different Temperatures (L, long period; x_{CL}, linear degree of crystallinity; Q, invariant; l_C (the product of L and x_{CL}), lamellar thickness)

T, °C	Q, a.u.	L, Å	x_{CL}, %	l_C, Å
320	5.5	146	70.4	103
330	5.6	158	71.1	112
340	5.3	152	71.2	108
350	7.6	164	71.4	117
360	5.5	152	71.6	109

in spherulites formed at lower temperatures, in which a spiral line initiated from the center of the spherulite can be seen. At higher crystallization temperatures, as the ring spacing is coarsened, the spiral line becomes very irregular. Figure 12 shows a TEM micrograph of the etched surface from the ringed spherulites formed at a low crystallization temperature. Although the chosen etching condition was not optimized to reveal the detailed surface texture, the ringed texture is apparent. The width of the ring was estimated to be *ca*. 400 nm, and the thickness, *ca*. 100 nm.

There appears to be a correlation between the ring formation, the concentration of the flexible alkyl (C12) chains, and the temperature. If we assume the ringed textures result from the twisted lamellae, then such a morphology may only become stable when the chain flexibility is high. Perhaps, this is because, at the low

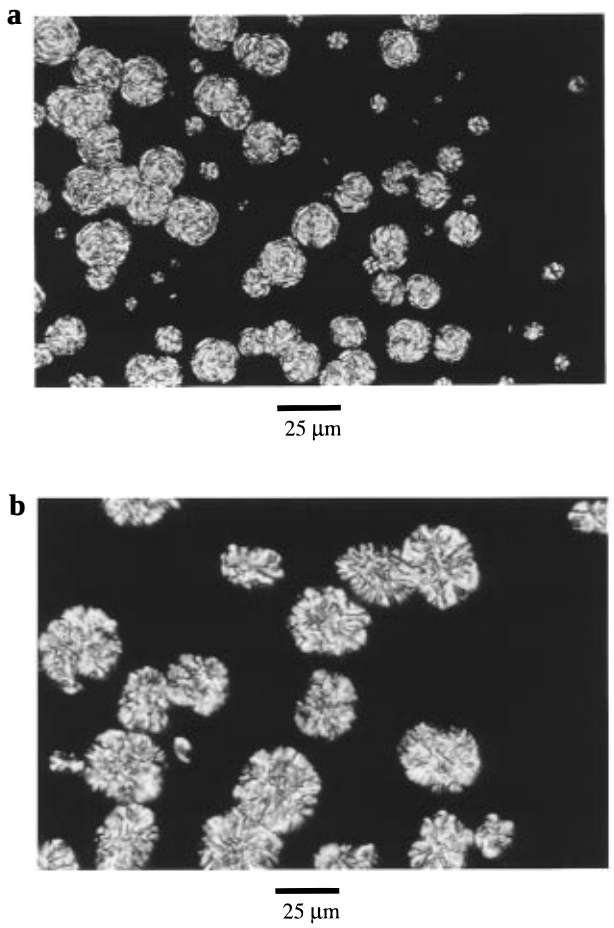

Figure 11. Polarizing optical micrographs of ringed spherulites from C12/BPDA samples: (a) spherulites formed at 165 °C; (b) spherulites formed at 200 °C.

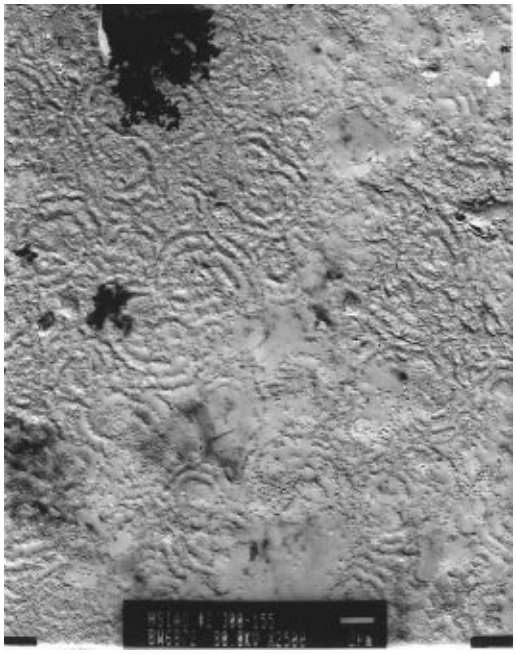

Figure 12. TEM micrograph of a replica from etched C12/BPDA PI surfaces (crystallized at 180 °C) showing the ringed texture.

concentration of C12, the ringed spherulite could only occur at high temperatures where the chain is more flexible. As the temperature decreases and the chain rigidity increases, the ringed spherulite formation may become nonfavorable.

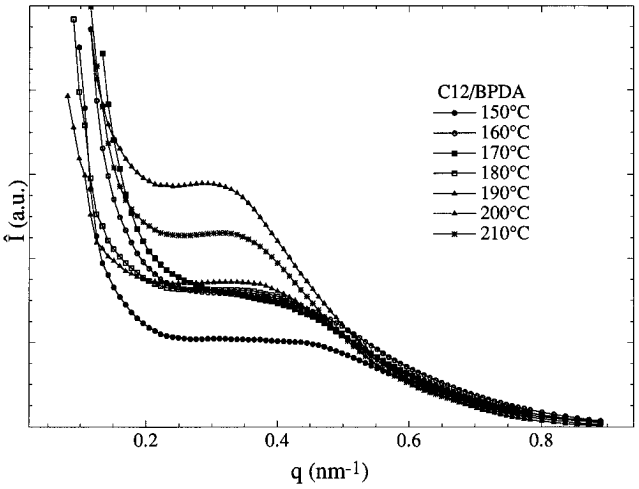

Figure 13. SAXS patterns (with smeared intensity) taken from C12/BPDA samples crystallized at different temperatures.

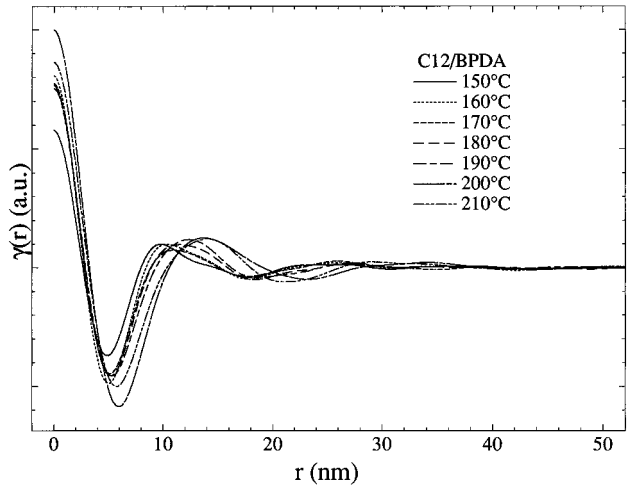

Figure 14. Corresponding correlation function diagrams calculated from Figure 13.

Table 2. Lamellar Variables Calculated by Correlation Functions $\gamma(r)$ (Figure 14) from C12/BPDA Samples Crystallized at Different Temperatures

T, °C	Q, a.u.	L, Å	x_{CL}, %	l_C, Å
150	1.6	98	68.1	67
160	2.2	103	69.1	71
170	2.1	109	69.8	76
180	2.1	115	69.5	80
190	2.1	124	69.4	86
200	2.8	138	70.3	97
210	2.5	141	71.3	100

We believe the ringed spherulites also consist of lamellar crystals, even though it has not been revealed by TEM observations, since SAXS patterns taken from the crystalline C12/BPDA samples exhibit a consistent scattering maximum (Figure 13). The corresponding diagrams for the correlation function are shown in Figure 14, from which we have again calculated different lamellar variables. The results of these variables are listed in Table 2. It is seen that the long period listed here is much smaller than that in 134APB/BPDA (Table 1). Consequently, the lamellar thickness also becomes narrower (in the range 7−9 nm) than that of 134APB/BPDA. But it is found to increase with the crystallization temperature. The values of Q in Table 2 are lower than those in Table 1, which can be due to the low electron density contrast in the C12/BPDA system.

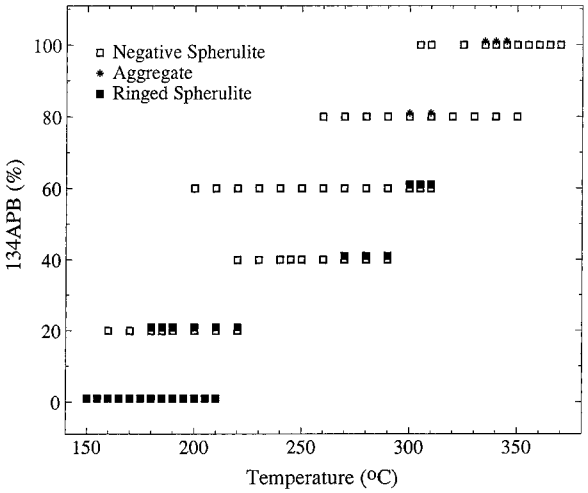

Figure 15. Summary of three different spherulite morphologies in polymers with different diamine compositions at different temperatures.

In copolyimides, different spherulite types are often found to coexist at some measuring temperatures. We have summarized the spherulite morphology as functions of composition and temperature in Figure 15. It is found that with the increasing C12 ratio, the polymers exhibit a wider temperature window to form ringed spherulites. This window always appears at higher crystallization temperatures. At lower crystallization temperatures, the spherulites are Maltese-cross like with a negative birefringence. The coexistence of the negative and the ringed spherulites is indicative of the phase separation induced by crystallization of different species.

Conclusion

In this work, we have studied the crystallization, melting, and morphology of a copolyimide family containing 3,3′,4,4′-biphenyltetracarboxylic dianhydride (BPDA) and either 1,3-bis(4-aminophenoxy)benzene (134APB) or 1,12-dodecanediamine (C12) monomers. It was seen that the crystallization and melting behavior in the compositions from 100/0 to 40/60 was dominated by the 134APB/BPDA crystals, and the behavior in the compositions of 20/80 to 0/100 was dominated by the C12/BPDA crystals. In the compositions of 40/60 and 20/80, a mixed behavior was seen, as evident by the dual minima in the crystallization peak time curve. The bulk crystallization rate was found to be significantly reduced by the presence of a minority phase, whereas the corresponding change in the growth rate was relatively small. This indicates that the change in the bulk crystallization rate was primarily due to the reduction in nucleation density. The highest endotherm in the triple-melting behavior is found to be rate dependent, which must be associated with a recrystallization or reorganization process rather than the polymorphism. Three types of spherulite morphologies have been identified in this copolyimide family: (1) typical Maltese-cross spherulites with negative birefringence which were seen in most compositions having high 134APB/BPDA content; (2) aggregate-like spherulites which were only observed in the compositions of 100/0 and 80/20 at temperatures having the maximum growth rate; (3) ringed spherulites which were seen in the compositions with high C12/BPDA contents and at higher

crystallization temperatures. Both Maltese-cross spherulites and ringed spherulites contain lamellar crystals, whose dimensions were estimated by SAXS and correlation function methods to be in the range of 10−12 nm for 134APB/BPDA and 6−10 nm for C12/BPDA.

Acknowledgment. The authors wish to thank J. P. McKeown and J. E. Freida for their technical assistance. Special thanks are given to Dr. K. H. Gardner for the WAXD measurement, Dr. B. A. Wood for the TEM measurement, and Dr. F. C. Wilson for the SAXS measurement.

References and Notes

(1) Kreuz, J. A.; Hsiao, B. S.; Renner, C. A.; Goff, D. L. *Macromolecules* **1995**, *28*, 6926.
(2) Cheng, S. Z. D.; Heberer, D. P.; Janimak, J. P.; Lien, S. H. S.; Harris, F. W. *Polymer* **1991**, *32* (11), 2053.
(3) Cheng, S. Z. D.; Heberer, D. P.; Lien, S. H. S.; Harris, F. W. *J. Polym. Sci., Polym. Phys. Ed.* **1990**, *28*, 655.
(4) Heberer, D. P.; Cheng, S. Z. D.; Barley, J. S.; Lien, S. H. S.; Bryant, R. G.; Harris, F. W. *Macromolecules* **1991**, *24*, 1890.
(5) Martuscelli, E., Palumbo, R., Kryszewski, M., Eds. *Polymer Blends, Processing, Morphology and Properties*; Plenum Press: New York, 1979; Vol. 1.
(6) Kryszewski, M., Galeski, A., Martuscelli, E., Eds. *Polymer Blends, Processing, Morphology and Properties*; Plenum Press: New York, 1979; Vol. 2.
(7) Klempner, D., Frisch, K. C., Eds. *Polymer Alloys*; *Polymer Alloys II*; Plenum Press: New York, 1979.
(8) Olabisi, O.; Mobeson, L. M.; Shaw, M. T. *Polymer-Polymer Miscibility*; Academic Press: New York, 1979.
(9) Guinier, A.; Fournet, G. *Small-Angle Scattering of X-Rays*; Chapman & Hall: London, 1955.
(10) Santa Cruz, C.; Stribeck, N.; Zachmann, H. G.; Bálta Calleja, F. J. *Macromolecules* **1991**, *24*, 5980.
(11) Wunderlich, B. *Macromolecular Physics*; Academic Press: New York, 1976; Vol. 2.
(12) Gardner, K. H.; Hsiao, B. S.; Matheson, R. R.; Wood, B. A. *Polymer* **1991**, *33*, 2483.
(13) Meeten, G. H. *Optical Properties of Polymers*; Elsevier: New York, 1986.
(14) Lovinger, A.; Davis, D. D. *Macromolecules* **1986**, *19*, 1861.
(15) Lovinger, A.; Davis, D. D. *J. Appl. Phys.* **1985**, *58* (8), 2843.
(16) Bassett, D. C.; Olley, R. H.; Al Raheil, I. A. M. *Polymer* **1988**, *29*, 1745.
(17) MaGill, J. H. *J. Polym. Sci., Polym. Phys. Ed.* **1966**, *4*, 243.
(18) Clark, E. S.; Wilson, F. C. In *Nylon Plastics*; Kohan, M. I., Ed.; John Wiley & Sons: New York, 1973; Chapter 8.

MA950459R